Neurobiology of Disease

Intracellular Accumulation of Amyloid-β (Aβ) Protein Plays a Major Role in Aβ-Induced Alterations of Glutamatergic Synaptic Transmission and Plasticity

Cristian Ripoli,[1]* Sara Cocco,[1]* Domenica D. Li Puma,[1] Roberto Piacentini,[1] Alessia Mastrodonato,[1] Federico Scala,[1] Daniela Puzzo,[2] Marcello D'Ascenzo,[1] and Claudio Grassi[1]

[1]Institute of Human Physiology, Università Cattolica, 00168 Rome, Italy and [2]Department of Bio-Medical Sciences–Section of Physiology, University of Catania, 95125 Catania, Italy

Intracellular accumulation of amyloid-β (Aβ) protein has been proposed as an early event in AD pathogenesis. In patients with mild cognitive impairment, intraneuronal Aβ immunoreactivity was found especially in brain regions critically involved in the cognitive deficits of AD. Although a large body of evidence demonstrates that Aβ42 accumulates intraneuronally ($_{in}$Aβ), the action and the role of Aβ42 buildup on synaptic function have been poorly investigated. Here, we demonstrate that basal synaptic transmission and LTP were markedly depressed following Aβ42 injection into the neuron through the patch pipette. Control experiments performed with the reverse peptide (Aβ42-1) allowed us to exclude that the effects of $_{in}$Aβ depended on changes in oncotic pressure. To further investigate $_{in}$Aβ synaptotoxicity we used an Aβ variant harboring oxidized methionine in position 35 that does not cross the neuronal plasma membrane and is not uploaded from the extracellular space. This Aβ42 variant had no effects on synaptic transmission and plasticity when applied extracellularly, but induced synaptic depression and LTP inhibition after patch-pipette dialysis. Finally, the injection of an antibody raised against human Aβ42 (6E10) in CA1 pyramidal neurons of mouse hippocampal brain slices and autaptic microcultures did not, per se, significantly affect LTP and basal synaptic transmission, but it protected against the toxic effects of extracellular Aβ42. Collectively, these findings suggest that Aβ42-induced impairment of glutamatergic synaptic function depends on its internalization and intracellular accumulation thus paving the way to a systemic proteomic analysis of intracellular targets/partners of Aβ42.

Key words: **6E10; amyloid-β protein; autaptic hippocampal neurons; intraneuronal accumulation; synaptic transmission; whole-cell LTP**

Introduction

Amyloid-β (Aβ) oligomers have been proposed to be key mediators of cognitive decline in AD (Selkoe, 2002). Aβ induces synaptotoxicity regardless of the genetic predisposition to this pathology (Li et al., 2013). Indeed, brain slices of *wt* mice exposed to nanomolar concentrations of human Aβ showed impaired hippocampal LTP (Malenka and Malinow, 2011; Li et al., 2013), that is the cellular correlate of memory (Bliss and Collingridge, 1993; Nabavi et al., 2014). Many studies have proposed that Aβ oligomers exert their synaptotoxic effects by binding to membrane receptors thereby affecting molecular pathways involved in neuronal functions responsible for the transmission and storage of information in the brain (Parihar and Brewer, 2010; Benilova et al., 2012; Benilova and De Strooper, 2013). However, to date pharmacological approaches targeting these receptors have not yet led to effective treatments for preventing and/or delaying the disease progression (Small et al., 2007; Bonda et al., 2010). While several studies have investigated the effects of Aβ on neuronal membrane receptors and the intracellular pathways activated downstream, the hypothesis that Aβ42 internalization from the extracellular space and its intraneuronal accumulation are critical to Aβ42-dependent synaptotoxicity has not been fully tested yet. Notably, in the early phases of AD (i.e., mild cognitive impairment and prodromal AD), intraneuronal accumulation of Aβ was found especially in brain regions critically involved in the cognitive deficits (LaFerla et al., 2007). Moreover, the largest known genetic risk factor for late-onset sporadic AD, i.e., the ApoE4 isoform of ApoE gene, significantly increased Aβ accumulation in neurons compared with the protective ApoE2 variant (Kuszczyk et al., 2013). There is also evidence that intraneuronal Aβ accumulation contributes to tau hyperphosphorylation (Takahashi et al., 2010), reduces synaptic protein expression (Almeida et al., 2005), and induces mitochondrial dysfunction (Lustbader et al., 2004; Zepa et al., 2011). We recently demonstrated that 20 min of extracellular application of 200 nM Aβ42 decreased mEPSC frequency and vesicular release probability in autaptic hippocampal neurons without significantly affecting the postsynaptic compartment (Ripoli et al.,

Received March 25, 2014; revised July 25, 2014; accepted Aug. 15, 2014.

Author contributions: C.R. and C.G. designed research; C.R., S.C., D.D.L.P., R.P., A.M., F.S., and M.D. performed research; C.R., S.C., D.D.L.P., R.P., F.S., D.P., and M.D. analyzed data; C.R. and C.G. wrote the paper.

This work was supported by grants from Università Cattolica to C.G. and from Alzheimer's Association (NIRG-14-321307) to C.R.

*C.R. and S.C. contributed equally to this work.

The authors declare no competing financial interests.

Correspondence should be addressed to Claudio Grassi, Institute of Human Physiology, Università Cattolica, Largo Francesco Vito 1, 00168 Rome, Italy. E-mail: grassi@rm.unicatt.it.

DOI:10.1523/JNEUROSCI.1201-14.2014

 0270-6474/14/3412893-11$15.00/0

2013). We speculated that presynaptic alterations represent the earliest dysfunction followed by frank synapse loss. Here we report that intracellular accumulation of Aβ dramatically affects glutamatergic synaptic function at both presynaptic and postsynaptic levels. Our findings suggest that synaptotoxicity of Aβ may occur independently of its interaction with plasma membrane receptors, and that Aβ42 internalization from the extracellular space and its intracellular accumulation play a pivotal role in synaptic dysfunction.

Materials and Methods

All animal procedures were approved by the Ethics Committee of the Catholic University and University of Catania, complied with Italian Ministry of Health guidelines and with national laws (Legislative decree 116/1992) and European Union guidelines on animal research (No. 86/609/EEC).

Preparation of amyloid solutions. Freeze-dried purified Aβ40, Aβ42, Aβ42-1, and Aβ42 variant harboring oxidized methionine at position 35 ($A\beta42^{MO}$) and human amylin were purchased from AnaSpec. Protein solutions were prepared as previously described (Piacentini et al., 2008a; De Chiara et al., 2010; Maiti et al., 2011; Attar et al., 2012; Ripoli et al., 2013) according to standard procedures. Briefly, peptides were diluted to 1 mM in 1,1,1,3,3,3,-hexafluoro-2-propanol to disassemble preformed aggregates and stored as dry films at −20°C before use. The films were dissolved at 1 mM in DMSO, sonicated for 10 min, diluted to 100 μM in cold PBS, and incubated for 12–18 h at 4°C to promote protein oligomerization. The final working concentrations (1–1000 nM) were obtained by diluting the 100 μM amyloid proteins in extracellular or intracellular solutions (for salts composition, see below). The same amount of DMSO/PBS contained in Aβ42 solutions was used as vehicle. In some experiments, Aβ diluted in internal solution was subjected to 0.22 μm filtration (Minisart; Sartorius Stedim Biotech).

Western immunoblotting for Aβ42. Protein solutions were analyzed by Western blotting as previously described with minor modification (De Stefano et al., 2005; Attar et al., 2012; Ripoli et al., 2013). Briefly, in SDS-PAGE analysis the Aβ samples (final concentration of 200 nM) were mixed with NuPAGE LDS sample buffer 4× and separated on 10–20% gradient Novex Tricine precast gels (Invitrogen) according to the manufacturer's protocol. After electrophoresis the proteins were transferred to 0.2 μm nitrocellulose membranes (GE Healthcare). Membranes were blocked for 1 h, at room temperature (RT; 22−24°C), in a suspension of 5% nonfat milk in Tris-buffered saline containing 0.1% Tween 20 before incubation overnight at 4°C with mouse monoclonal antibody 6E10 (1:1000; Covance). Membranes were washed three times with Tris-buffered saline containing 0.1% Tween 20 and then incubated with HRP-conjugated anti-mouse secondary antibody (1:2000; Cell Signaling Technology) at RT for 1 h. Protein expression was evaluated by using the Super Signal West Femto chemiluminescence kit (Pierce). Immunoblots were documented by using UVItec Cambridge Alliance. Experiments were performed in triplicate.

Primary hippocampal neuron cultures. Hippocampal neurons from P0 to P2 C57BL/6 mice, eGFP-expressing mice (Okabe et al., 1997) or B6.129S7-App^{tm1Dbo}/J mice (APP knock-out mice purchased from The Jackson Laboratory) brains were prepared according to standard procedure as previously described (Piacentini et al., 2008b; Ripoli et al., 2013) with some modifications. Briefly, hippocampi were incubated for 10 min at 37°C in PBS containing trypsin-EDTA (0.025%/0.01% w/v; Biochrom AG), and the tissue was mechanically dissociated at RT with a fire-polished Pasteur pipette. The cell suspension was harvested and centrifuged at 235 × *g* for 8 min. The pellet was suspended in 88.8% MEM (Biochrom), 5% fetal bovine serum, 5% horse serum, 1% glutamine (2 mM), 1% penicillin-streptomycin-neomycin antibiotic mixture (Invitrogen), and glucose (25 mM). Cells were plated at a density of 1×10^5 cells on 20 mm coverslips precoated with poly-L-lysine (0.1 mg/ml; Sigma). Twenty-four hours later, the culture medium was replaced with a mixture of 96.5% Neurobasal medium (Invitrogen), 2% B-27 (Invitrogen), 0.5% glutamine (2 mM), and 1% penicillin-streptomycin-neomycin antibiotic mixture. After 72 h, this medium was replaced with a glutamine-free version of the same medium, and the cells were grown for 10 more days before experiments.

Electrophysiology in autaptic microcultures. Autaptic hippocampal neurons were prepared as previously described (Attar et al., 2012; Ripoli et al., 2013). To create microislands where glial cells could be grown, a mixture of poly-D-lysine and collagen (both from Sigma) was sprayed on agarose-coated glass coverslips. Cortical astrocytes from the brains of P0–P2 C57BL/6 mice (grown for 1 week in DMEM supplemented with 10% fetal bovine serum and antibiotics) were plated onto the coverslips (Podda et al., 2012). After 4–6 d, the medium was conditioned before neuron plating by replacing half the medium volume with neuronal medium (consisting of Neurobasal medium, 2% B-27, 0.5% glutamine, and 1% penicillin-streptomycin-neomycin antibiotic mixture). Hippocampal neurons from P0 to P2 C57BL/6 and B6.129S7-App^{tm1Dbo}/J mice were prepared as described above and suspended in neuronal medium. Later, neurons were plated onto glial microislands at low density ($25{,}000/cm^2$) to obtain a ratio of one neuron per island. Every 4 d half the neuronal medium volume was replaced with fresh neuronal medium supplemented with 2 μM cytosine arabinoside. Autapses were studied from 9 to 21 DIV.

Basal synaptic transmission was studied using the patch-clamp technique in the whole-cell configuration as previously described (Attar et al., 2012; Ripoli et al., 2013). Recordings were obtained with an Axopatch 200B amplifier (Molecular Devices), and stimulation and data acquisition were performed with the Digidata 1200 series interface and pCLAMP 10 software (Molecular Devices). Patch electrodes, fabricated from borosilicate glass capillaries with the aid of a micropipette puller (P-97; Sutter Instruments) had resistances of 3–5 MΩ when filled with the internal solution that contained the following (in mM): 146 K-gluconate, 18 HEPES, 1 EGTA, 4.6 $MgCl_2$, 4 NaATP, 0.3 Na_2GTP, 15 creatine phosphate, and 5 U/ml phosphocreatine kinase. For recordings, cells were constantly perfused with an external Tyrode's solution containing the following (in mM): 140 NaCl, 2 KCl, 10 HEPES, 10 glucose, 4 $MgCl_2$, and 4 $CaCl_2$, pH 7.4, 312 mOsm. We monitored the access resistance and membrane capacity before and at the end of the experiments to ensure recording stability and the health of studied cells. Recordings were considered stable when the series and input resistances, resting membrane potential, and stimulus artifact duration did not change >20%. Comparisons were performed between data collected after whole-cell configuration had been achieved (referred as T_0) and 20 min later (referred as T_{20}).

EPSCs were recorded in autaptic neurons voltage clamped at a membrane potential of −70 mV, with stimuli mimicking action potentials (2 ms at 0 mV) delivered every 10 s or 20 s. NMDA currents were evoked using Mg-free Tyrode's solution containing 10 μM of the AMPA receptor blocker NBQX (Tocris Bioscience). To obtain the AMPA:NMDA ratio, evoked responses were always recorded successively from the same cell. The amplitude and frequency of spontaneous mEPSCs were evaluated in 60 s recordings. The detection threshold was set to 3.5 times the baseline SD. The size of the readily releasable vesicle pool (RRP) of synaptic vesicles was estimated by measuring the charge induced by increasing the transmembrane osmotic pressure in the presynaptic terminal by a 4 s extracellular application of hypertonic (0.5 M) sucrose solution. The total RRP charge was then estimated as the integral of the fast, transient inward current component, after subtraction of the steady-state component. RRP refilling was investigated in paired-pulse experiments, in which 0.5 M sucrose solution was applied for 4 s at 4 s interpulse intervals. The RRP recovery rate was expressed as the peak amplitude of the second response normalized to that of the first response. To evaluate short-term plasticity, EPSCs were recorded from neurons stimulated at 20 Hz (Ting et al., 2006). The decay time constant (τ) was measured by fitting the normalized EPSC amplitude plot of each cell with monoexponential function (Origin 5.0 software; OriginLab). The paired-pulse ratio (PPR) consisted of the ratio of the amplitude of the second EPSC to that of the first recorded in 20 Hz trains. Steady-state values were evaluated by averaging EPSC amplitudes in response to 30–40th stimuli. All experiments were performed at RT.

Electrophysiology in hippocampal brain slices. All experiments were performed with 21-d-old male C57BL/6 mice. Animals were anesthetized

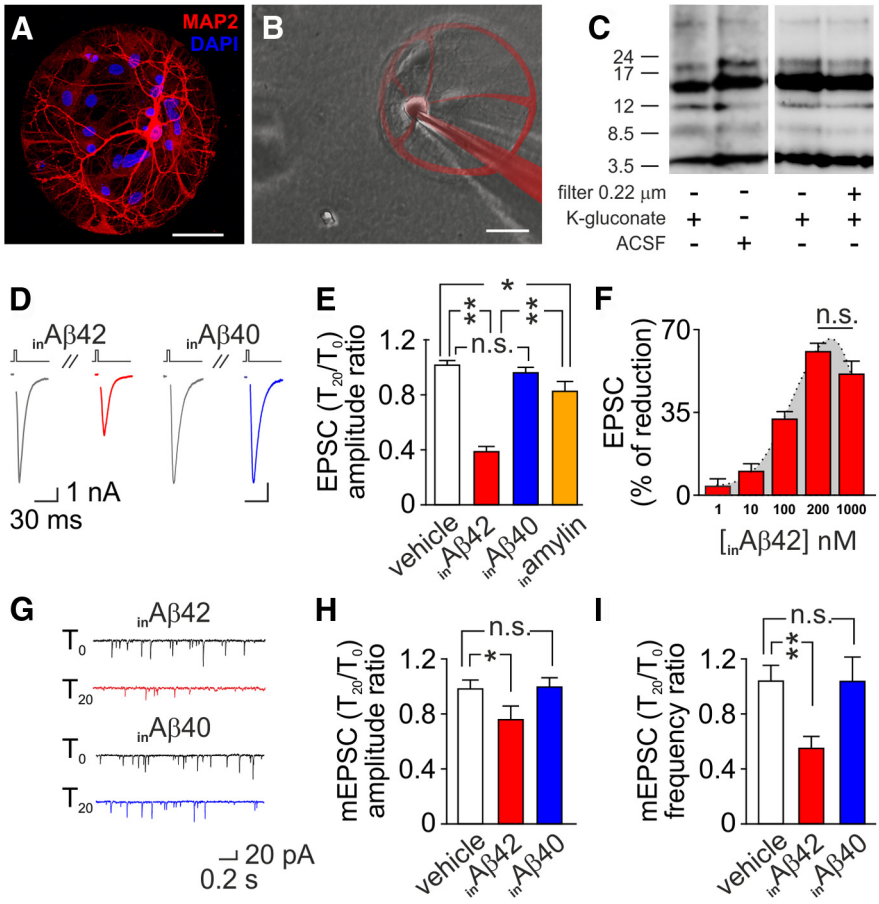

Figure 1. Accumulation of $_{in}$Aβ plays a major role in Aβ-induced alterations of glutamatergic synaptic function. ***A***, Representative image of a hippocampal autaptic culture. Red staining for MAP2 identifies the single neuron grown onto glial microisland. Blue staining (DAPI) identifies cell nuclei. ***B***, Image depicting intracellular application of 200 nM Aβ42. ***C***, Representative Western blot of Aβ oligomer distribution in ACSF and unfiltered or 0.22 μm filtered K-gluconate solution. None of the above described experimental conditions markedly affected Aβ42 small oligomer distribution. ***D***, Representative traces of EPSC currents at T_0 (gray lines) and after 20 min intracellular application of 200 nM Aβ42 (red line) or 200 nM Aβ40 (blue line). Stimulus artifacts for EPSC currents were removed for clarity. ***E***, Bar graphs (mean ± SEM) showing the T_{20}/T_0 ratio of EPSC amplitude in autaptic neurons exposed to vehicle (white bar), $_{in}$Aβ42 (red bar), $_{in}$Aβ40 (blue bar), or amylin (orange bar). ***F***, Dose–response relationship of $_{in}$Aβ42 effects on EPSC amplitude. ***G***, Representative traces of mEPSC currents at T_0 (gray lines) and T_{20} with 200 nM $_{in}$Aβ42 (red line) or 200 nM $_{in}$Aβ40 (blue line). Bar graphs (mean ± SEM) showing the T_{20}/T_0 ratio of mEPSC amplitude (***H***) and frequency (***I***) in autaptic neurons exposed to vehicle (white bars), $_{in}$Aβ42 (red bars), or $_{in}$Aβ40 (blue bars). Scale bars: ***A***, ***B***, 50 μm. *$p < 0.05$; **$p < 0.005$; n.s.: $p > 0.05$.

with isoflurane and decapitated. The brains were rapidly removed and placed in ice-cold cutting solution containing the following (in mM): 124 NaCl, 3.2 KCl, 1 NaH_2PO_4, 2 $MgCl_2$, 1 $CaCl_2$, 26 $NaHCO_3$, 10 glucose, 2 Na-pyruvate, and 0.6 ascorbic acid, pH 7.4, 95% O_2/5% CO_2. Slices (300 μm thick) were cut on a vibratome (VT1000S; Leica Microsystems) and immediately transferred to an incubation chamber filled with ACSF containing the following (in mM): 124 NaCl, 3.2 KCl, 1 NaH_2PO_4, 1 $MgCl_2$, 2 $CaCl_2$, 26 $NaHCO_3$, and 10 glucose, pH 7.4, 95% O_2/5% CO_2. The slices were allowed to recover at 32°C for 1 h before being equilibrated at RT. For electrophysiological recordings, slices were transferred to a submerged recording chamber constantly perfused with heated ACSF (32°C) and bubbled with 95% O_2/5% CO_2 (Podda et al., 2008; Fusco et al., 2012).

Experiments examining LTP were performed from single CA1 pyramidal cells after stimulating the Schaffer collateral fibers by means of a bipolar tungsten electrode (Warner Instruments). All recordings were made with the $GABA_A$ receptor antagonist picrotoxin (50 μM) added to the ACSF. Whole-cell recording pipettes (3–5 MΩ) were filled with a solution containing the following (in mM): 135 $CsMeSO_3$, 8 NaCl, 10 HEPES, 0.25 EGTA, 2 Mg_2ATP, 0.3 Na_3GTP, 0.1 spermine, 7 phosphocreatine, and 5 QX-314, pH 7.25–7.30, 294–298 mOsm. Data were collected with a Multiclamp 700A amplifier (Molecular Devices). A Digidata 1440 series interface and pClamp 10 software (Molecular Devices) were used for data acquisition and stimulation protocols. Data were filtered at 1 kHz, digitized at 10 kHz, and analyzed on-line and off-line. Hippocampal subfields and electrode positions were identified with the aid of 4× and 40× water-immersion objectives on an upright microscope equipped with differential interference contrast optics under infrared illumination (BX5IWI; Olympus) and video observation (C3077-71 CCD camera; Hamamatsu Photonics).

To study LTP in CA1 pyramidal cells, the amplitudes of EPSCs elicited by stimulation of Schaffer collateral fibers were measured. The stimulation intensity that elicited one-third of the maximal response was used for delivering test pulses every 20 s. During recordings, CA1 pyramidal cells were held at −60 mV to record AMPA receptor-mediated EPSCs. LTP was induced by two trains of HFS (100 Hz, 1 s) separated by 20 s, while cells were depolarized to 0 mV. This induction protocol was always applied within 5–7 min of achieving whole-cell configuration, to avoid "wash-out" of LTP. Responses to test pulse were recorded for 30 min to assess LTP. The amplitudes of EPSC at 30 min were averaged from values obtained during the last 5 min of post-HSF recordings (from minute 25 to minute 30). LTP magnitude was expressed as the percentage change in the mean EPSC peak amplitude normalized to baseline values = 100% (i.e., mean values for the 5 min of recording before HFS). Unless otherwise specified, all commercial products were used according to manufacturers' instructions.

Study of Aβ internalization. To study internalization of Aβ42, both *wt* and $Aβ42^{MO}$ were labeled with the IRIS 5-NHS active ester dye (IRIS 5; λ_{ex}: 633 nm, λ_{em}: 650–700 nm; Cyanine Technology) as previously described (Ripoli et al., 2013). IRIS 5 dye is suitable for conjugation of any biomolecules carrying free primary amines, such as proteins and peptides. Briefly, Aβ solutions (100 μM in PBS) were mixed with 6 mM IRIS 5 in DMSO for 4 h in the dark under mild shaking conditions. After this time, labeled Aβs were purified with Vivacon 500 ultrafiltration spin columns (2 kDa cutoff; Sartorius Stedim Biotech) and then resuspended in PBS at a concentration of 100 μM before final dilution in the culture medium.

Time-dependent internalization of IRIS 5-labeled Aβ42 (either *wt* or $Aβ42^{MO}$) was then studied by time-lapse confocal imaging in hippocampal neurons derived from eGFP-expressing mice or by immunocytochemistry in hippocampal neurons derived from C57BL/6 mice.

Immunocytochemistry. Hippocampal neurons cultured for 15 DIV and treated with IRIS 5-labeled Aβ42 analogs were fixed with 4% paraformaldehyde (Sigma) in PBS for 15 min at RT. After being permeabilized (15 min incubation with 0.3% Triton X-100 in PBS; Sigma), cells were incubated for 20 min with 0.3% BSA in PBS to block nonspecific binding sites and then overnight at 4°C with mouse antimicrotubule-associated protein 2 (MAP2; 1:300, Sigma). For experiments aimed at evaluating the effects of Aβ42 on synaptic proteins, neuronal cultures were fixed and permeabilized as previously described, and then incubated overnight with either mouse anti-PSD-95 (1:250; Abcam) or rabbit monoclonal anti-synaptophysin (1:250; Abcam) and mouse anti-MAP2. The next day, cells were incubated for 90 min at RT with Alexa Fluor 488 donkey

anti-mouse or donkey anti-rabbit and/or Alexa Fluor 546 donkey anti-mouse antibodies (1:1000; Invitrogen). Nuclei were counterstained with DAPI (0.5 μg/ml for 10 min; Invitrogen), and finally cells were coverslipped with ProLong Gold antifade reagent (Invitrogen).

Images (512 × 512 or 1024 × 1024 pixels) were acquired at 63× magnification with a confocal laser scanning system (TCS-SP2; Leica) and an oil-immersion objective (NA 1.4). DAPI staining was imaged after two-photon excitation with an ultrafast, tunable mode-locked titanium:sapphire laser (Chameleon; Coherent).

Immunofluorescence for synaptophysin and PSD-95 was quantified as the sum of fluorescence intensities (8-bit depth) measured for every pixel in the recorded field. For synaptophysin, we also calculated the "protein density", i.e., the total fluorescence intensity of synaptophysin labeling divided by the total area in the field that was occupied by neurons (identified by MAP2 immunoreactivity). The operator was blind to the study conditions.

Immunohistochemistry and biocytin labeling. To study dendritic spine density, patch-clamped CA1 neurons in hippocampal slices were dialyzed with the intracellular solutions containing 0.2% biocytin (Sigma) and either 200 nM $_{in}$Aβ42 or vehicle. After 20 min of whole-cell dialysis, slices were fixed overnight at 4°C with 0.1 M PBS containing 4% paraformaldehyde. After fixation, slices were incubated for 60 min in blocking solution containing 10% normal goat serum and 0.3% Triton X-100 (Sigma) in PBS. Subsequently, biocytin was revealed by incubating slices with Alexa Fluor 488-conjugated avidin (1:500 in blocking solution; Life Technologies) for 90 min at RT. Slices were then washed three times in PBS, mounted with ProLong Gold antifade reagent (Life Technologies), and finally studied with a high-resolution confocal microscope (Leica TCS-SP2).

Spines were imaged with a 63× magnification objective (NA 1.40) plus additional magnification of 5×. Images were taken at 1024 × 1024 pixel resolution (physical pixel size: 46 nm). Spine density was analyzed under blinded conditions in randomly chosen segments (length: 40–43 μm) of secondary dendrites from apical branches and expressed as the number of spines per 100 μm dendrites. A total length of at least 1.2 mm was analyzed for each experimental condition.

Apoptosis assays. Apoptosis was evaluated in hippocampal cultures with the APO-BrdU TUNEL assay Kit (Invitrogen) according to the manufacturer's instructions, as described in Podda et al. (2014). Briefly, the cell cultures were exposed to 200 nM Aβ42 or vehicle for 1 h. Cells exposed for 3 h to 100 μM H_2O_2 were used as positive control of apoptosis. Apoptotic cells were identified immunocytochemically by means of anti-BrdU antibody labeled with Alexa Fluor 488 dye, whereas cell nuclei were identified by means of propidium iodide. Images (512 × 512 pixels) were obtained at 40× magnification with a high-resolution confocal microscope (Leica TCS-SP2).

In some cultures, the intermediate stages of apoptosis were also investigated by annexin V staining (FITC conjugated; Life Technologies).

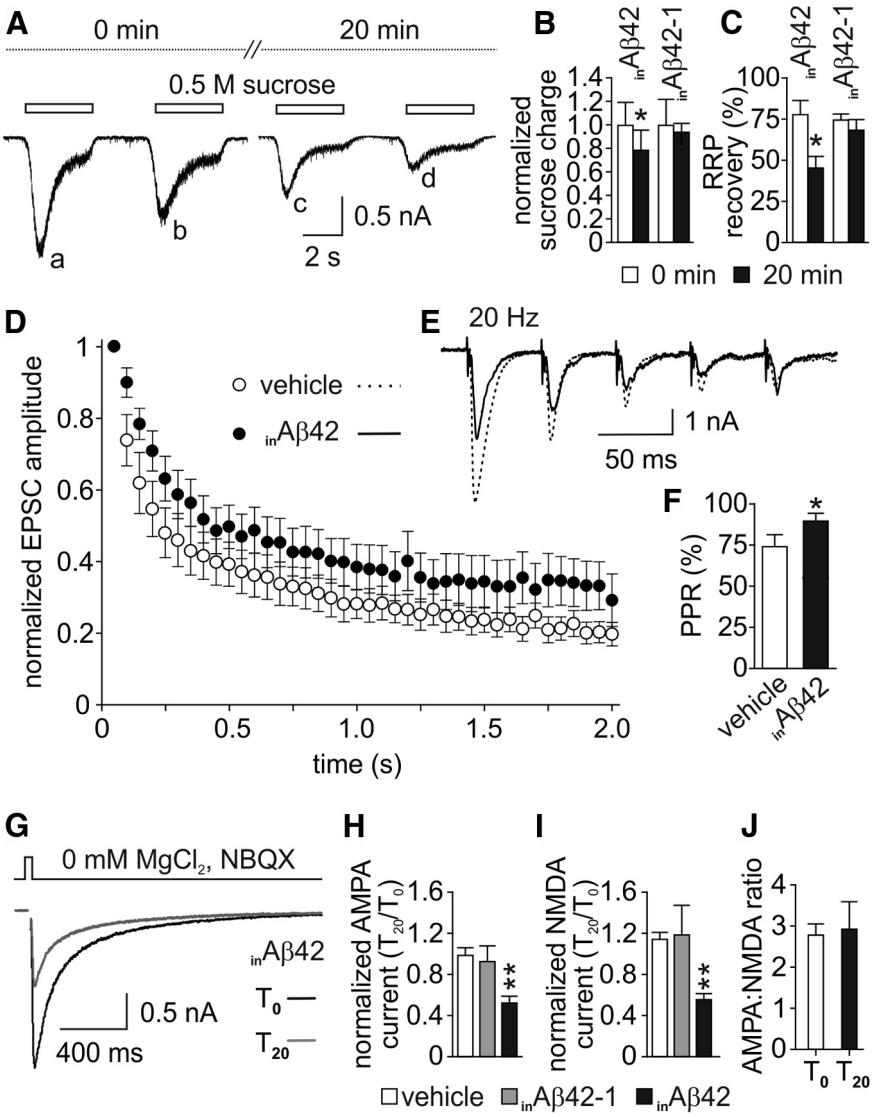

Figure 2. Intracellular application of Aβ42 markedly affects glutamatergic synaptic transmission. ***A***, Representative traces of paired-pulse currents induced by 4 s applications of 0.5 M sucrose (4 s interpulse intervals) at T_0 and T_{20} of $_{in}$Aβ42. Following Aβ42 injection (trace c collected at T_{20}) the sucrose charge was markedly lower than at T_0 (trace a). ***B***, Bar graphs (mean ± SEM) showing the normalized sucrose charge at T_0 (white bars) and T_{20} (black bars) in $_{in}$Aβ42- or $_{in}$Aβ42-1-injected neurons. ***C***, Bar graphs (mean ± SEM) showing the RRP recovery rate expressed as the peak amplitude of the second responses normalized to that of the first response at T_0 (b/a in ***A***; white bars) and T_{20} (d/c in ***A***; black bars) in $_{in}$Aβ42- or $_{in}$Aβ42-1-injected neurons. ***D***, EPSC amplitudes normalized to the first response during 2 s trains at 20 Hz. ***E***, Representative traces of the first five responses evoked by trains of stimuli (20 Hz) after 20 min of vehicle or $_{in}$Aβ42 applications. ***F***, Mean PPRs after 20 min of vehicle or $_{in}$Aβ42 application. ***G***, Representative traces of NMDA currents (stimulus artifacts removed for clarity) at T_0 (black line) and T_{20} (gray line) with $_{in}$Aβ42. Bar graphs (mean ± SEM) showing the T_{20}/T_0 ratio of AMPA (***H***) and NMDA (***I***) currents with vehicle (white bars), $_{in}$Aβ42-1 (gray bars), and $_{in}$Aβ42 (black bars). ***J***, Bar graphs (mean ± SEM) showing the AMPA:NMDA ratio at T_0 and T_{20} with $_{in}$Aβ42. *$p < 0.05$; **$p < 0.01$.

Statistical analysis. All data are shown as mean ± SEM. Statistical analyses (Student's paired and unpaired *t* tests) were performed with SYSTAT 10.2 software (Statcom). The level of significance was set at 0.05.

Results

Intracellular application of Aβ42 markedly affected glutamatergic synaptic transmission

In autaptic hippocampal neurons we studied the effects of intracellular application of Aβ42 ($_{in}$Aβ42), injected into neurons through the patch pipette (Fig. 1*A*,*B*). First, we checked whether the different composition of intrapipette and extracellular solutions we used for patch-clamp experiments affected Aβ42 oligomerization. Western

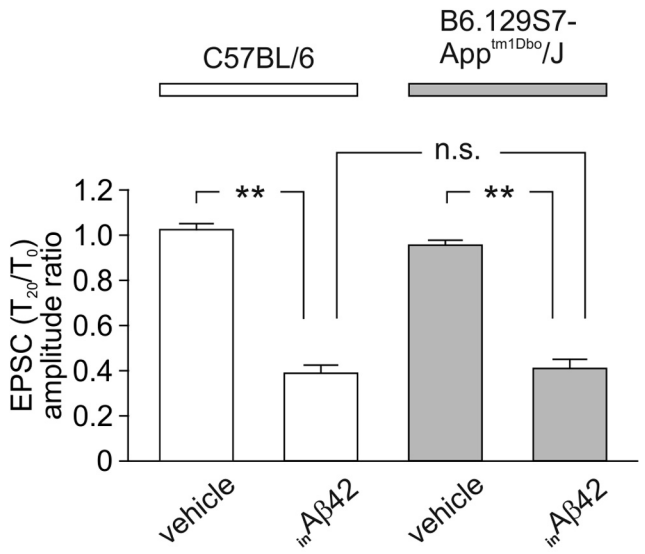

Figure 3. EPSC amplitude inhibition induced by $_{in}$Aβ42 is independent of its interaction with either APP or APP cleavage products. Bar graphs (mean ± SEM) showing the T_{20}/T_0 ratio of EPSC amplitude in autaptic neurons derived from C57BL/6 (white bars) and B6.129S7-App^{tm1Dbo}/J mice (APP knock-out mice; gray bars) exposed to either vehicle or 200 nM $_{in}$Aβ42. $^{**}p < 0.005$; n.s.: $p > 0.05$.

blot analysis showed similar Aβ oligomer distribution in the different solutions used (Fig. 1*C*). Synaptic strength was quantified by measuring the amplitude of action potential-evoked EPSCs along with mEPSC amplitude and frequency. EPSC amplitudes were markedly depressed after 20 min (T_{20}) application of 200 nM $_{in}$Aβ42 (T_{20} vs T_0: −62.3 ± 3.1%; $n = 24$; $p < 0.005$; Fig. 1*D*,*E*), whereas after 20 min intracellular application of vehicle we found no significant changes in EPSC amplitudes ($p = 0.38$; $n = 22$; Fig. 1*E*).

To determine the specificity of $_{in}$Aβ42 effects we also loaded neurons with either 200 nM Aβ40, another most common isoform of Aβ, or 200 nM Aβ42-1 with the same molecular weight and amino acid composition of Aβ1–42 but assembled in the reverse mode. Neither Aβ40 nor Aβ42-1 significantly affected EPSC amplitudes [T_{20} vs T_0: $p = 0.49$ ($n = 10$) and 0.75 ($n = 11$), respectively; Fig. 1*D*,*E*]. Although Aβ42-1 shares with Aβ1–42 the same molecular weight and amino acid composition, neither this reverse peptide nor Aβ40 exhibit the same tendency of Aβ42 to oligomerize. We then performed further control experiments with amylin, an amyloid protein that differs from Aβ42 in its primary sequence but shares with it the ability to oligomerize (Lorenzo et al., 2000). As expected on the basis of previous studies (Kimura et al., 2012), we found that 20 min intracellular application of 200 nM amylin decreased EPSC amplitude by 17.6 ± 6.5% ($p < 0.05$; $n = 11$; Fig. 1*E*). However, such decrease was significantly lower than that caused by 200 nM $_{in}$Aβ42 ($_{in}$Aβ42 vs $_{in}$amylin; $p < 0.005$).

Dose–response relationship was studied by using $_{in}$Aβ42 concentrations ranging from 1 to 1000 nM (Fig. 1*F*), which are in the same range of intracellular Aβ42 concentrations reported in neurons of AD models (Hu et al., 2009; Hashimoto et al., 2010). The lowest concentration causing a statistically significant decrease in EPSC amplitude was 10 nM (−9.1 ± 4.3%; $n = 21$; $p < 0.01$). Higher $_{in}$Aβ42 concentrations produced more marked effects reaching a plateau at 200 nM. Indeed, no significant differences were found between EPSC amplitude decreases observed at 200 and 1000 nM ($p = 0.11$; Fig. 1*F*).

As shown in Figure 1*G–I*, exposure to $_{in}$Aβ42 decreased both mEPSC amplitude (T_{20} vs T_0: −23.5 ± 10.9%; $n = 16$; $p < 0.05$) and frequency (−44.8 ± 8.4%; $n = 16$; $p < 0.005$). Neither vehicle ($n = 15$) nor 200 nM $_{in}$Aβ40 ($n = 10$) significantly modified these parameters (Fig. 1*G–I*). In a set of experiments aimed at investigating in greater detail the effects of $_{in}$Aβ42 on synaptic transmission, we challenged neurons with 0.5 M sucrose solution to measure the RRP at T_0 and 20 min after $_{in}$Aβ42 loading (Fig. 2*A*). Upon locally puffing 0.5 M sucrose for 4 s onto the recorded autaptic neuron, a transient current reflecting glutamate release from docked vesicles was observed (Fig. 2*A*). The response to this hypertonic stimulus was significantly smaller after 20 min $_{in}$Aβ42 application than at T_0 (−23.7 ± 8.4%; $p < 0.05$; $n = 8$; Fig. 2*A*, compare traces c and a, *B*). Paired stimuli of hypertonic sucrose solution, delivered at 4 s intervals, revealed a decreased refilling rate of the RRP after 20 min $_{in}$Aβ42 application (T_0: 78.3 ± 9.0%; T_{20}: 45.8 ± 6.5%; $n = 8$; $p < 0.05$; Fig. 2*A*,*C*), likely reflecting a reduced vesicle number and/or vesicular release probability within terminals. Control experiments performed with 200 nM $_{in}$Aβ42-1 did not reveal significant changes in either sucrose charge or RRP recovery ($n = 8$; $p = 0.71$ and 0.16, respectively; Fig. 2*B*,*C*). Moreover, we estimated the vesicular release probability and the short-term plasticity within these synapses by using a train of 40 stimuli at 20 Hz (Fig. 2*D–F*). The kinetics of EPSC amplitude depression was significantly slower after 20 min $_{in}$Aβ42 application relative to controls: the mean decay time constants (τ) of monoexponential functions fitting the normalized EPSC amplitude plots were 380 ± 72 ms in Aβ42-injected neurons and 220 ± 33 ms in controls ($n = 15$; $p < 0.05$). This finding suggests a reluctance of synapses in Aβ42-filled neurons to deplete the RRP vesicles. Release probability was investigated by analyzing the PPR between the firsts two stimuli of the abovementioned 20 Hz paradigm that was significantly increased by $_{in}$Aβ42 ($p < 0.05$; Fig. 2*D–F*). These data suggest a significant decrease of release probability in Aβ42-injected neurons compared with controls.

As shown in Figure 2, *G* and *I*, NMDA currents were also significantly reduced 20 min after 200 nM $_{in}$Aβ42 (−44.2 ± 6.5%, $n = 10$; $p < 0.01$). In this set of experiments, we restricted our study to NMDA receptor- and AMPA receptor-mediated EPSC amplitudes without investigating other electrophysiological parameters to minimize the risk of current run-down occurring in long-lasting recordings. In the same neuron we first recorded the synaptically evoked NMDA currents followed by AMPA receptor-mediated EPSCs, both at T_0 and T_{20}. After 20 min $_{in}$Aβ42 the decrease in NMDA current amplitude was very similar to that observed in AMPA currents (−44.2 ± 6.5% and −47.6 ± 6.4%, respectively; Fig. 2*H*,*I*). This finding was confirmed by studying the AMPA:NMDA ratio that was unaltered in hippocampal autapses after Aβ42 loading via the patch pipette (Fig. 2*J*).

Literature reports suggested that Aβ toxicity may be mediated by its binding to APP (Lorenzo et al., 2000; Shaked et al., 2006). To check whether the diminished neurotransmission induced by $_{in}$Aβ42 depended of its interaction with either APP or APP cleavage products including Aβ42 physiologically present in neurons, we performed patch-clamp recordings in autaptic hippocampal APP-null neurons loaded with 200 nM Aβ42. The EPSC amplitude inhibition induced by $_{in}$Aβ42 in this experimental model (−58.1 ± 2.8%; $n = 17$; $p < 0.005$; Fig. 3) was not significantly different from that observed in hippocampal neurons from *wt* mice.

Finally, we checked whether $_{in}$Aβ42 synaptotoxicity was due to specific early synaptic effects rather than to cell death/damage or frank synapse loss. To this aim we studied: (1) dendritic spine density in hippocampal neurons of brain slices loaded with both

Aβ42 and biocytin and (2) expression of synaptic proteins (synaptophysin and PSD-95) and apoptosis (annexin V immunoreactivity and TUNEL assay) in hippocampal neuronal cultures treated for 60 min with vehicle or Aβ42. As shown in Figure 4, *A–C*, 20 min intracellular application of 200 nM Aβ42 did not significantly affect dendritic spine density (79 ± 4 and 77 ± 5 spines per 100 μm with vehicle and 200 nM $_{in}$Aβ42, respectively; $p = 0.65$). Moreover, study of annexin V immunoreactivity and TUNEL assay did not reveal signs of cell death/damage in neurons exposed for 60 min to extracellular Aβ42 (data not shown). Noteworthy, as described in greater detail below, cell-culture exposure to 200 nM Aβ42 for 60 min was associated with significant Aβ42 internalization and intraneuronal accumulation. Finally, the same treatment did not significantly affect synaptophysin and PSD-95 immunoreactivity (data not shown).

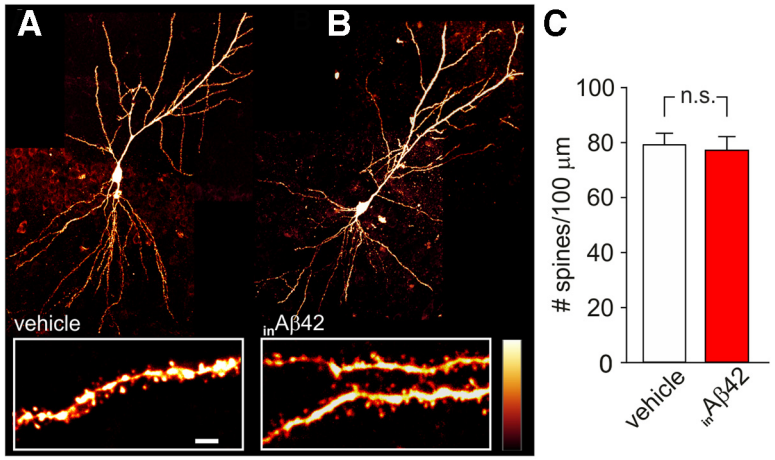

Figure 4. Twenty minute injection of Aβ42 does not significantly affect dendritic spine density of CA1 hippocampal neurons. ***A***, ***B***, Representative examples of CA1 neurons filled with biocytin and revealed with avidin conjugated to Alexa Fluor 488. Neuron shown in ***A*** was injected with vehicle, whereas neuron shown in ***B*** was injected with 200 nM Aβ42 for 20 min. Bottom boxes in ***A*** and ***B*** show high-magnification images of dendritic segments of cells in ***A*** and ***B***, respectively. Scale bar, 3 μm. Alexa Fluor 488 fluorescence intensity (8-bit depth) was represented according to the color scale on the right (bottom = 0, top = 256). ***C***, Bar graphs showing the mean number of dendritic spines per 100 μm. n.s.: $p > 0.05$.

Hippocampal LTP was markedly inhibited by $_{in}$Aβ42

To investigate the effects of $_{in}$Aβ42 on synaptic plasticity, in acute hippocampal brain slices we studied LTP at CA3–CA1 synapses by applying LTP protocols within 5–7 min after achieving whole-cell configuration (see Materials and Methods). Under control conditions, i.e., when hippocampal slices were perfused with vehicle alone or Aβ42-1 was injected into CA1 pyramidal neurons, the EPSC amplitude recorded 30 min after HFS displayed increases of 119.7 ± 17.8% ($n = 8$) and 127.0 ± 30.1% ($n = 8$), respectively (Fig. 5*A*,*B*). LTP was markedly lower when neurons were loaded with 200 nM Aβ42 through the patch pipette (14.9 ± 18.7%; $n = 8$; $p < 0.005$; Fig. 5*A*,*B*).

An Aβ42 variant, unable to be uploaded intraneuronally, had no effects on synaptic transmission and plasticity when applied extracellularly but induced synaptic depression and LTP inhibition after patch-pipette dialysis

Numerous papers, including ours, demonstrated that extracellularly applied Aβ42 ($_{ex}$Aβ42) markedly affects synaptic transmission and plasticity (Pettit et al., 2001; Wei et al., 2010; Jo et al., 2011; Attar et al., 2012; Li et al., 2013; Ripoli et al., 2013). We hypothesized that neuronal uploading of $_{ex}$Aβ42 from extracellular space and its intracellular accumulation are critical determinants of its synaptotoxicity. To test this hypothesis, we labeled Aβ42 with the fluorescent dye IRIS 5-NHS and studied its localization by high-resolution confocal microscopy. We found that, when applied extracellularly, Aβ42 crossed the neuronal membrane and was internalized both at somatic and dendritic levels during the 20 min application (Fig. 6*A*,*B*), which is the time frame of our electrophysiological recordings. We then looked for Aβ variants exhibiting biophysical properties comparable to those of *wt*Aβ but unable to cross plasma membrane and be uploaded intraneuronally. In previous studies we demonstrated that Aβ42^{MO} exhibited soluble small-oligomer distribution similar to that of *wt*Aβ but very limited neurotoxicity (Piacentini et al., 2008a; Ripoli et al., 2013). This Aβ variant scarcely crossed the neuronal membrane: after 20 min application most of the labeled

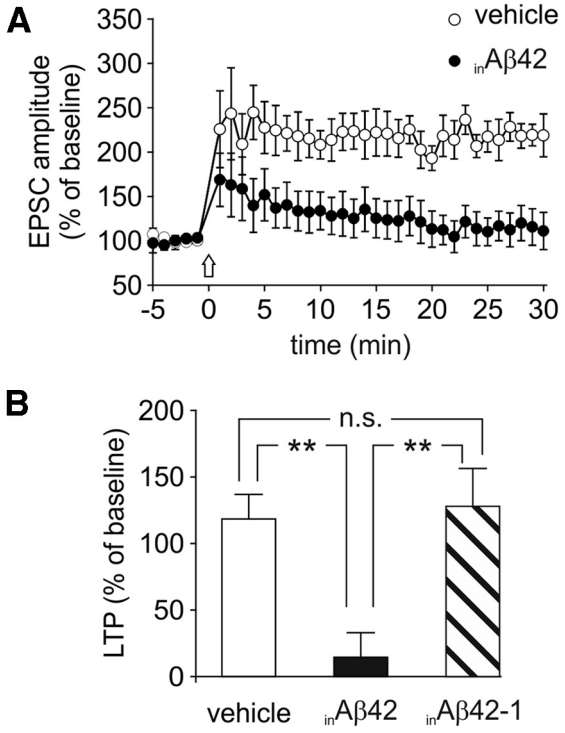

Figure 5. LTP is markedly inhibited by $_{in}$Aβ42. ***A***, Time course of EPSC amplitudes before and after HFS (indicated by arrow) in hippocampal brain slices treated with vehicle (white circles) and $_{in}$Aβ42 (black circles). ***B***, Bar graphs (mean ± SEM) showing the EPSC amplitudes measured during the last 5 min of recording under the conditions described for ***A*** and during the last 5 min of $_{in}$Aβ42-1. **$p < 0.005$; n.s.: $p > 0.05$.

Aβ42^{MO} was confined outside the cells, as also shown by the *X-Z* cross sections from the *Z*-stack acquisitions (Fig. 6*C*). Therefore, Aβ42^{MO} was a very useful tool to further investigate the role of $_{in}$Aβ42 in synaptic dysfunction. In autaptic microcultures exposed to extracellularly applied Aβ42^{MO} ($_{ex}$Aβ42^{MO}, 200 nM), no significant changes in either evoked EPSC amplitudes (T_{20} vs T_0: $p = 0.10$; $n = 9$; Fig. 6*D*) or mEPSC amplitude and frequency ($p = 0.92$ and $p = 0.36$, respectively; $n = 7$; Fig. 6*E*,*F*) were

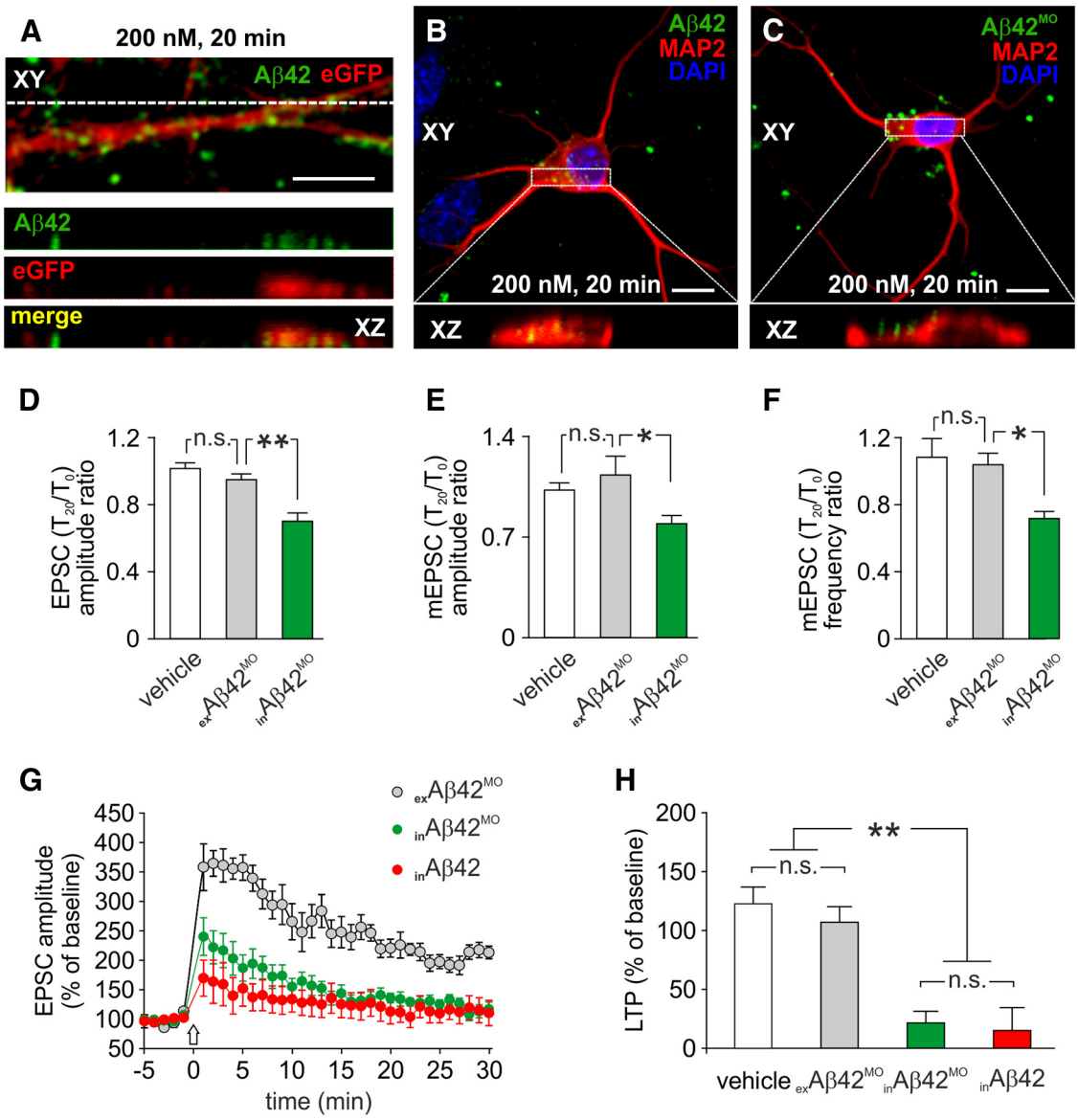

Figure 6. Extracellular Aβ42^{MO} has no effects on synaptic transmission and plasticity but induces synaptic depression and LTP inhibition after patch-pipette dialysis. ***A***, Representative example of a dendrite from eGFP^{+} hippocampal neuron (red) following 20 min extracellular application of 200 nM IRIS 5-labeled Aβ42 (green). Representative examples of neurons exposed for 20 min to 200 nM IRIS 5-labeled Aβ42 (***B***) and Aβ42^{MO} (***C***). Red staining indicates MAP2 immunoreactivity. Bottom boxes in ***A–C*** represent *X-Z* cross sections from the *Z*-stack acquisitions showing the different neuronal accumulation of Aβ42 analogs after 20 min treatments. Bar graphs comparing the T_{20}/T_0 ratio of EPSC amplitude (***D***), mEPSC amplitude (***E***), and mEPSC frequency (***F***) measured in autaptic neurons following application of vehicle (white bars), $_{ex}$Aβ42^{MO} (gray bars), and $_{in}$Aβ42^{MO} (green bars). ***G***, Time course of EPSC amplitudes before and after HFS (indicated by arrow) in hippocampal slices treated with $_{ex}$Aβ42^{MO} (gray circles), $_{in}$Aβ42^{MO} (green circles), and $_{in}$Aβ42 (red circles). ***H***, Bar graphs (mean ± SEM) showing the EPSC amplitudes measured during the last 5 min of recording under the conditions described for ***G*** and during the last 5 min of vehicle. Scale bars: ***A–C***, 10 μm. *$p < 0.05$; **$p < 0.005$; n.s.: $p > 0.05$.

observed. Of note, 20 min after intracellular application of 200 nM Aβ42^{MO} ($_{in}$Aβ42^{MO}) both EPSC and mEPSC were significantly changed (EPSC: −30.4 ± 4.0%; $n = 17$; $p < 0.005$; mEPSC amplitude: −20.7 ± 5.7%; $n = 12$; $p < 0.05$; mEPSC frequency: −28.4 ± 3.9%; $n = 12$; $p < 0.05$; Fig. 6*D–F*). These findings indicate that intraneuronal uploading of soluble Aβ oligomers is critical for Aβ-mediated depression of basal synaptic transmission.

To determine whether intraneuronal accumulation was also required for Aβ42-induced LTP inhibition, we examined the effects of $_{ex}$Aβ42^{MO} and $_{in}$Aβ42^{MO} in hippocampal brain slices. Extracellular application of 200 nM Aβ42^{MO} had no effects on synaptic plasticity: LTP was 106.6 ± 12.3% ($n = 8$) and 119.7 ± 17.8% ($n = 8$), with $_{ex}$Aβ42^{MO} and vehicle, respectively (Fig. 6*G*,*H*). On the contrary, this Aβ variant inhibited LTP to a similar level of *wt* $_{in}$Aβ42 when applied via the patch pipette (21.5 ± 9.5%; $n = 10$; $p < 0.005$ vs vehicle; Fig. 6*G*,*H*).

Effects of $_{ex}$Aβ42 on synaptic dysfunction likely depended on its ability to accumulate intraneuronally

To further investigate the role of intracellular accumulation of Aβ42 and its internalization from extracellular space in the synaptic dysfunction, we tested the effects of $_{ex}$Aβ42 on EPSCs, mEPSCs, and LTP after loading the recorded neurons with an antibody raised against human Aβ42 (6E10; 1:300). This antibody recognizes the sequence 1–16 of human Aβ42 (Tampellini et al., 2007) and, therefore, it counteracts the action of human synthetic Aβ42 we used in our experiments. Injection of 6E10

into CA1 pyramidal neurons through the patch pipette ($_{in}$6E10) did not, per se, significantly affect LTP (132.4 ± 24.9%, $n = 9$), but it protected against the toxic effects of $_{ex}$Aβ42: LTP recorded with $_{ex}$Aβ42 + $_{in}$6E10 and $_{ex}$Aβ42 alone were 104.8 ± 16.3% ($n = 9$) and 66.2 ± 12.6% ($n = 8$; $p < 0.01$ vs vehicle), respectively ($_{ex}$Aβ42+ $_{in}$6E10 vs $_{ex}$Aβ42; $p < 0.05$; Fig. 7*A*,*B*). These findings clearly suggested that internalization of $_{ex}$Aβ42 is critical to LTP inhibition induced by Aβ42. We performed similar experiments in autaptic neurons and we found that $_{in}$6E10 counteracted the alterations of basal synaptic transmission induced by $_{ex}$Aβ42 in terms of both EPSC amplitude ($_{ex}$Aβ42 + $_{in}$6E10 vs $_{ex}$Aβ42; $p < 0.05$) and mEPSC frequency ($_{ex}$Aβ42 + $_{in}$6E10 vs $_{ex}$Aβ42; $p < 0.05$; $n = 15$; Fig. 7*C*–*E*).

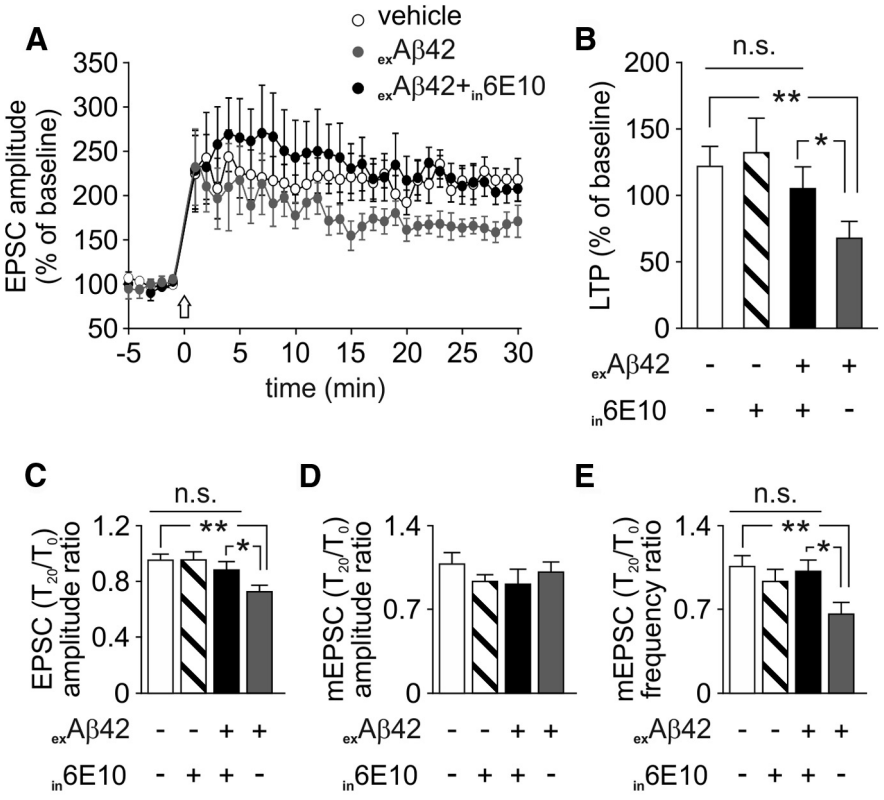

Figure 7. Inhibition of hippocampal LTP and basal synaptic transmission induced by $_{ex}$Aβ42 likely depends of its ability to be uploaded intraneuronally. ***A***, Time course of EPSC amplitudes before and after HFS (indicated by arrow) in hippocampal slices treated with vehicle (white circles), $_{ex}$Aβ42 (gray circles), and $_{ex}$Aβ42 + $_{in}$6E10 (black circles). ***B***, Bar graphs (mean ± SEM) showing the EPSC amplitudes measured during the last 5 min of recording under the conditions described for ***A*** and during the last 5 min of $_{in}$6E10 alone. Bar graphs comparing the T_{20}/T_0 ratio of EPSC amplitude (***C***), mEPSC amplitude (***D***), and mEPSC frequency (***E***) measured in autaptic neurons following application of vehicle (white bars), $_{in}$6E10 (striped bars), $_{ex}$Aβ42 + $_{in}$6E10 (black bars), and $_{ex}$Aβ42 (gray bars). *$p < 0.05$; **$p < 0.01$; n.s.: $p > 0.05$.

Discussion

Intraneuronal accumulation of Aβ is emerging as a key determinant of AD pathogenesis because it has been proposed to play a critical role in synaptic dysfunction underlying the cognitive impairment observed in AD (Gouras et al., 2000, 2010, 2012; Billings et al., 2005; LaFerla et al., 2007; Moreno et al., 2009; Bayer and Wirths, 2010; Nomura et al., 2012; Eimer and Vassar, 2013). However, most of these studies relied on molecular findings. Functional studies demonstrated that in squid giant synapses intraneuronal Aβ reduced the rate of rise of EPSPs that, eventually, became subthreshold for action potential generation (Moreno et al., 2009). These effects were attributed to diminished docked synaptic vesicles in Aβ42-microinjected terminals with no significant changes in the clathrin-coated vesicles (Nomura et al., 2012). However, the synaptic dysfunction caused by intraneuronal Aβ in glutamatergic mammalian neurons and the underlying mechanisms are far from being fully understood. Our study investigated the contribution of intracellular accumulation of Aβ42 to alterations of glutamatergic synaptic transmission and plasticity focusing on Aβ42 internalization as a critical event in its synaptotoxicity. In particular, our paper demonstrates that Aβ42 uploading from the extracellular space and its intracellular accumulation dramatically affect a number of functional synaptic parameters. A major advantage of our approach is that we tested the effects of an Aβ42 variant unable to cross plasma membranes and studied the effects of $_{ex}$Aβ42 after neuronal loading with an antibody raised against human Aβ42. Collectively, the results of these experiments allowed us to elucidate the role of $_{in}$Aβ42 in synaptic dysfunction. Of note, the intracellular application of Aβ42 through patch pipette bypassed and ruled out mechanisms and/or intracellular pathways activated by Aβ binding to membrane receptors.

Many literature reports have suggested that Aβ42 binding to membrane receptors affects molecular mechanisms governing synaptic function. Aβ-mediated synaptotoxicity was attributed to activation of the metabotropic glutamate receptors, mGluR5, and stimulation of three kinases, JNK1, Cdk5, and p38 MAPK, mediating LTP inhibition (Wang et al., 2004). Moreover, Aβ has been reported to interact with α7-containing nicotinic acetylcholine receptors (nAChRs; Wang et al., 2000; Dineley et al., 2001; Liu et al., 2001; Pettit et al., 2001). Glutamate release was reportedly affected by Aβ via inhibition of presynaptic nAChR (Dougherty et al., 2003). Aβ was also suggested to trigger NMDA receptor internalization following nAChR activation (Snyder et al., 2005). Moreover, Aβ binding to receptors for advanced glycation end products (RAGE) mediated MAPK phosphorylation leading to synaptic dysfunction (Origlia et al., 2009a,b). Aβ oligomers have also been reported to bind the fibronectin repeats domain of EphB2 and trigger EphB2 degradation causing deficits in learning and memory (Cissé et al., 2011). More recently, Kim et al. (2013) identified two new receptors for Aβ: the murine PirB and its human ortholog LilrB2 whose activation triggered a signaling cascade affecting the actin cytoskeleton and causing synaptic loss. Finally, experimental evidence suggests that APP itself is required for extracellular Aβ signaling (Lorenzo et al., 2000; Shaked et al., 2006).

Definitely, a number of molecular pathways activated by membrane receptors have been proposed to underlie Aβ42-induced synaptic dysfunction. However, our findings allow us to hypothesize that synaptic dysfunction primarily depends on direct Aβ42 interaction with intracellular partners. In our view Aβ42 binding to membrane receptors might play a key role in Aβ internalization rather than directly triggering intracellular molecular pathways leading to synaptic dysfunction. Indeed, the

NMDA receptor antagonist AP5 completely blocked Aβ42 internalization (Bi et al., 2002), which was facilitated by Aβ42 binding to α7-nAChRs, followed by endocytosis of the resulting complex (Nagele et al., 2002).

Our confocal microscopy experiments documented that $_{ex}$Aβ42 was rapidly internalized and accumulated at both somatic and dendritic levels. Hence, we asked whether the effects of $_{ex}$Aβ42 depended on its ability to cross the plasma membrane. We found that, in autaptic hippocampal neurons, 20 min of $_{ex}$Aβ42 selectively altered mEPSC frequency, i.e., the presynaptic vesicular release machinery (Ripoli et al., 2013), whereas $_{in}$Aβ42 affected both presynaptic and postsynaptic mechanisms. A biside effect of $_{ex}$Aβ42 was reported in APP-overexpressing neurons (Ting et al., 2007) and in autaptic microcultures exposed to $_{ex}$Aβ42 for longer (24–72 h) periods (Ripoli et al., 2013). We recently reported a time-dependent Aβ-induced alteration of glutamatergic synapses starting with changes in glutamate release and speculated that presynaptic alterations may represent the earliest step in synaptic dysfunction, followed by postsynaptic compartment impairment (Ripoli et al., 2013). Lipton's group recently confirmed Aβ-induced early synaptic injury consisting in decreased mEPSC frequency and suggested that the initial synaptic dysfunction, eventually followed by synapse loss, is due to excessive activation of extrasynaptic or perisynaptic NMDA receptors by glutamate released from astrocytes (Talantova et al., 2013). In our experimental model, the synaptic dysfunction caused by short-lasting Aβ42 applications was not associated to neuronal damage/death or synaptic loss, as documented by the results of TUNEL assay and immunoreactivity for annexin V, synaptophysin, and PSD-95. Our data suggest a model of Aβ42-induced synaptotoxicity including multiple presynaptic and postsynaptic mechanisms activated in a time-dependent manner. Of note, $_{ex}$Aβ42 has been shown to accumulate presynaptically and to directly compete with VAMP2 for binding to synaptophysin (Russell et al., 2012). Collectively, these results provide evidence that Aβ42 internalization is critical to deregulation of glutamatergic synapses.

We also found that $_{in}$Aβ42 markedly inhibited LTP at CA3–CA1 synapses. The effects of $_{in}$Aβ42 on LTP were recently investigated by Nomura et al. (2012) who did not find LTP inhibitions at $_{in}$Aβ42 concentrations >1 nM. Instead, we found that 200 nM $_{in}$Aβ42 produced a marked LTP inhibition whose specificity was documented by the absence of effects when 200 nM Aβ42-1 was injected into the studied neuron. A possible explanation of this discrepancy might depend on the different protocols we used for Aβ42 preparations. Indeed, Nomura et al. (2012) dissolved Aβ42 in DMSO and soon after they diluted it in the internal recording solution, whereas we induced Aβ oligomer formation by 12–18 h incubation at 4°C before experiments. These different protocols may markedly affect Aβ oligomerization as suggested by our mass spectrometry analyses revealing a prevalence of monomers when Aβ42-DMSO solutions were diluted in saline and studied within few hours (data not shown).

The marked effects of $_{in}$Aβ42 on basal synaptic transmission and LTP suggest that Aβ42 internalization is required to alter glutamatergic synapses. This conclusion was supported by the results of experiments performed with an Aβ variant, Aβ42^{MO}, which we previously demonstrated to exhibit soluble small-oligomer distribution similar to that of *wt*Aβ but is unable (1) to dysregulate Ca^{2+} currents, (2) to activate caspase-3 and induce apoptosis, (3) to markedly affect the expression of synaptic proteins and synaptic function, and (4) to cross the cell membrane (Clementi et al., 2006, Piacentini et al., 2008a; Maiti et al., 2011; Ripoli et al., 2013). Here we clearly demonstrated that the lack of synaptotoxic effects exhibited by Aβ42^{MO} depends on its inability to be uploaded intraneuronally. Indeed, Aβ42^{MO} does not affect synaptic transmission and plasticity when applied extracellularly but produces synaptic depression and LTP inhibition virtually identical to those caused by *wt*Aβ42 when it is injected into neurons via the recording electrode.

Further support to our contention that Aβ42 internalization and its intracellular accumulation are critical to Aβ42-induced synaptotoxicity came from the findings that injection of 6E10 antibody into the studied neuron blocked $_{ex}$Aβ42-dependent alterations of basal synaptic transmission and LTP. These findings suggest that Aβ42 synaptotoxicity occurs independently of intracellular pathways activated by Aβ42 interaction with membrane receptors. Molecular mechanisms leading to alterations of synaptic transmission and plasticity might primarily depend on Aβ interaction with intracellular molecular targets. Further studies are required to identify the causative events behind Aβ42 internalization and the intracellular interactors of Aβ42 that are responsible for its presynaptic and postsynaptic effects. A systemic proteomic analysis of intracellular Aβ42 partners will hopefully allow us to identify intraneuronal molecular targets useful to design novel drugs preventing and/or counteracting synaptic dysfunction and cognitive decline in AD.

References

Almeida CG, Tampellini D, Takahashi RH, Greengard P, Lin MT, Snyder EM, Gouras GK (2005) Beta-amyloid accumulation in APP mutant neurons reduces PSD-95 and GluR1 in synapses. Neurobiol Dis 20:187–198. CrossRef Medline

Attar A, Ripoli C, Riccardi E, Maiti P, Li Puma DD, Liu T, Hayes J, Jones MR, Lichti-Kaiser K, Yang F, Gale GD, Tseng CH, Tan M, Xie CW, Straudinger JL, Klärner FG, Schrader T, Frautschy SA, Grassi C, Bitan G (2012) Protection of primary neurons and mouse brain from Alzheimer's pathology by molecular tweezers. Brain 135:3735–3748. CrossRef Medline

Bayer TA, Wirths O (2010) Intracellular accumulation of amyloid-beta-a predictor for synaptic dysfunction and neuron loss in Alzheimer's disease. Front Aging Neurosci 2:8. CrossRef Medline

Benilova I, De Strooper B (2013) Neuroscience. Promiscuous Alzheimer's amyloid: yet another partner. Science 341:1354–1355. CrossRef Medline

Benilova I, Karran E, De Strooper B (2012) The toxic Aβ oligomer and Alzheimer's disease: an emperor in need of clothes. Nat Neurosci 15:349–357. CrossRef Medline

Bi X, Gall CM, Zhou J, Lynch G (2002) Uptake and pathogenic effects of amyloid beta peptide 1–42 are enhanced by integrin antagonists and blocked by NMDA receptor antagonists. Neuroscience 112:827–840. CrossRef Medline

Billings LM, Oddo S, Green KN, McGaugh JL, LaFerla FM (2005) Intraneuronal Aβ causes the onset of early Alzheimer's disease-related cognitive deficits in transgenic mice. Neuron 45:675–688. CrossRef Medline

Bliss TV, Collingridge GL (1993) A synaptic model of memory: long-term potentiation in the hippocampus. Nature 361:31–39. CrossRef Medline

Bonda DJ, Lee HP, Lee HG, Friedlich AL, Perry G, Zhu X, Smith MA (2010) Novel therapeutics for Alzheimer's disease: an update. Curr Opin Drug Discov Devel 13:235–246. Medline

Cissé M, Halabisky B, Harris J, Devidze N, Dubal DB, Sun B, Orr A, Lotz G, Kim DH, Hamto P, Ho K, Yu GQ, Mucke L (2011) Reversing EphB2 depletion rescues cognitive functions in Alzheimer model. Nature 469:47–52. CrossRef Medline

Clementi ME, Pezzotti M, Orsini F, Sampaolese B, Mezzogori D, Grassi C, Giardina B, Misiti F (2006) Alzheimer's amyloid β-peptide (1–42) induces cell death in human neuroblastoma via bax/bcl-2 ratio increase: an intriguing role for methionine 35. Biochem Biophys Res Commun 342:206–213. CrossRef Medline

De Chiara G, Marcocci ME, Civitelli L, Argnani R, Piacentini R, Ripoli C, Manservigi R, Grassi C, Garaci E, Palamara AT (2010) APP processing induced by herpes simplex virus type 1 (HSV-1) yields several APP fragments in human and rat neuronal cells. PLoS One 5:e13989. CrossRef Medline

De Stefano ME, Leone L, Lombardi L, Paggi P (2005) Lack of dystrophin leads to the selective loss of superior cervical ganglion neurons projecting to muscular targets in genetically dystrophic mdx mice. Neurobiol Dis 20:929–942. CrossRef Medline

Dineley KT, Westerman M, Bui D, Bell K, Ashe KH, Sweatt JD (2001) Beta-amyloid activates the mitogen-activated protein kinase cascade via hippocampal alpha7 nicotinic acetylcholine receptors: *in vitro* and *in vivo* mechanisms related to Alzheimer's disease. J Neurosci 21:4125–4133. Medline

Dougherty JJ, Wu J, Nichols RA (2003) Beta-amyloid regulation of presynaptic nicotinic receptors in rat hippocampus and neocortex. J Neurosci 23:6740–6747. Medline

Eimer WA, Vassar R (2013) Neuron loss in the 5XFAD mouse model of Alzheimer's disease correlates with intraneuronal Aβ42 accumulation and Caspase-3 activation. Mol Neurodegener 8:2. CrossRef Medline

Fusco S, Ripoli C, Podda MV, Ranieri SC, Leone L, Toietta G, McBurney MW, Schütz G, Riccio A, Grassi C, Galeotti T, Pani G (2012) A role for neuronal cAMP Responsive Element Binding (CREB)-1 in brain responses to calorie restriction. Proc Natl Acad Sci U S A 109:621–626. CrossRef Medline

Gouras GK, Tsai J, Naslund J, Vincent B, Edgar M, Checler F, Greenfield JP, Haroutunian V, Buxbaum JD, Xu H, Greengard P, Relkin NR (2000) Intraneuronal Aβ42 accumulation in human brain. Am J Pathol 156:15–20. CrossRef Medline

Gouras GK, Tampellini D, Takahashi RH, Capetillo-Zarate E (2010) Intraneuronal beta-amyloid accumulation and synapse pathology in Alzheimer's disease. Acta Neuropathol 119:523–541. CrossRef Medline

Gouras GK, Willén K, Tampellini D (2012) Critical role of intraneuronal Aβ in Alzheimer's disease: technical challenges in studying intracellular Aβ. Life Sci 91:1153–1158. CrossRef Medline

Hashimoto M, Bogdanovic N, Volkmann I, Aoki M, Winblad B, Tjernberg LO (2010) Analysis of microdissected human neurons by a sensitive ELISA reveals a correlation between elevated intracellular concentrations of Abeta42 and Alzheimer's disease neuropathology. Acta Neuropathol 119:543–554. CrossRef Medline

Hu X, Crick SL, Bu G, Frieden C, Pappu RV, Lee JM (2009) Amyloid seeds formed by cellular uptake, concentration, and aggregation of the amyloid-beta peptide. Proc Natl Acad Sci U S A 106:20324–20329. CrossRef Medline

Jo J, Whitcomb DJ, Olsen KM, Kerrigan TL, Lo SC, Bru-Mercier G, Dickinson B, Scullion S, Sheng M, Collingridge G, Cho K (2011) Aβ(1–42) inhibition of LTP is mediated by a signaling pathway involving caspase-3, Akt1 and GSK-3β. Nat Neurosci 14:545–547. CrossRef Medline

Kim T, Vidal GS, Djurisic M, William CM, Birnbaum ME, Garcia KC, Hyman BT, Shatz CJ (2013) Human LilrB2 is a β-amyloid receptor and its murine homolog PirB regulates synaptic plasticity in an Alzheimer's model. Science 341:1399–1404. CrossRef Medline

Kimura R, MacTavish D, Yang J, Westaway D, Jhamandas JH (2012) Beta amyloid-induced depression of hippocampal long-term potentiation is mediated through the amylin receptor. J Neurosci 32:17401–17406. CrossRef Medline

Kuszczyk MA, Sanchez S, Pankiewicz J, Kim J, Duszczyk M, Guridi M, Asuni AA, Sullivan PM, Holtzman DM, Sadowski MJ (2013) Blocking the interaction between apolipoprotein E and Aβ reduces intraneuronal accumulation of Aβ and inhibits synaptic degeneration. Am J Pathol 182:1750–1768. CrossRef Medline

LaFerla FM, Green KN, Oddo S (2007) Intracellular amyloid-β in Alzheimer's disease. Nat Rev Neurosci 8:499–509. CrossRef Medline

Li S, Jin M, Zhang D, Yang T, Koeglsperger T, Fu H, Selkoe DJ (2013) Environmental novelty activates β2-adrenergic signaling to prevent the impairment of hippocampal LTP by Aβ oligomers. Neuron 77:929–941. CrossRef Medline

Liu Q, Kawai H, Berg DK (2001) beta-Amyloid peptide blocks the response of alpha 7-containing nicotinic receptors on hippocampal neurons. Proc Natl Acad Sci U S A 98:4734–4739. CrossRef Medline

Lorenzo A, Yuan M, Zhang Z, Paganetti PA, Sturchler-Pierrat C, Staufenbiel M, Mautino J, Vigo FS, Sommer B, Yankner BA (2000) Amyloid beta interacts with the amyloid precursor protein: a potential toxic mechanism in Alzheimer's disease. Nat Neurosci 3:460–464. CrossRef Medline

Lustbader JW, Cirilli M, Lin C, Xu HW, Takuma K, Wang N, Caspersen C, Chen X, Pollak S, Chaney M, Trinchese F, Liu S, Gunn-Moore F, Lue LF, Walker DG, Kuppusamy P, Zewier ZL, Arancio O, Stern D, Yan SS, et al. (2004) ABAD directly links Aβ to mitochondrial toxicity in Alzheimer's disease. Science 304:448–452. CrossRef Medline

Maiti P, Piacentini R, Ripoli C, Grassi C, Bitan G (2011) Surprising toxicity and assembly behaviour of amyloid β-protein oxidized to sulfone. Biochem J 433:323–332. CrossRef Medline

Malenka RC, Malinow R (2011) Alzheimer's disease: recollection of lost memories. Nature 469:44–45. CrossRef Medline

Moreno H, Yu E, Pigino G, Hernandez AI, Kim N, Moreira JE, Sugimori M, Llinás RR (2009) Synaptic transmission block by presynaptic injection of oligomeric amyloid beta. Proc Natl Acad Sci U S A 106:5901–5906. CrossRef Medline

Nabavi S, Fox R, Proulx CD, Lin JY, Tsien RY, Malinow R (2014) Engineering a memory with LTD and LTP. Nature 511:348–352. CrossRef Medline

Nagele RG, D'Andrea MR, Anderson WJ, Wang HY (2002) Intracellular accumulation of beta-amyloid (1–42) in neurons is facilitated by the alpha 7 nicotinic acetylcholine receptor in Alzheimer's disease. Neuroscience 110:199–211. CrossRef Medline

Nomura I, Takechi H, Kato N (2012) Intraneuronally injected amyloid β inhibits long-term potentiation in rat hippocampal slices. J Neurophysiol 107:2526–2531. CrossRef Medline

Okabe M, Ikawa M, Kominami K, Nakanishi T, Nishimune Y (1997) 'Green mice' as a source of ubiquitous green cells. FEBS Lett 407:313–319. CrossRef Medline

Origlia N, Arancio O, Domenici L, Yan SS (2009a) MAPK, beta-amyloid and synaptic dysfunction: the role of RAGE. Expert Rev Neurother 9:1635–1645. CrossRef Medline

Origlia N, Capsoni S, Cattaneo A, Fang F, Arancio O, Yan SD, Domenici L (2009b) Abeta-dependent Inhibition of LTP in different intracortical circuits of the visual cortex: the role of RAGE. J Alzheimers Dis 17:59–68. CrossRef Medline

Parihar MS, Brewer GJ (2010) Amyloid-β as a modulator of synaptic plasticity. J Alzheimers Dis 22:741–763. CrossRef Medline

Pettit DL, Shao Z, Yakel JL (2001) β-Amyloid (1–42) peptide directly modulates nicotinic receptors in the rat hippocampal slice. J Neurosci 21:RC120. Medline

Piacentini R, Ripoli C, Leone L, Misiti F, Clementi ME, D'Ascenzo M, Giardina B, Azzena GB, Grassi C (2008a) Role of methionine 35 in the intracellular Ca^{2+} homeostasis dysregulation and Ca^{2+}-dependent apoptosis induced by amyloid β-peptide in human neuroblastoma IMR32 cells. J Neurochem 107:1070–1082. CrossRef Medline

Piacentini R, Gangitano C, Ceccariglia S, Del Fà A, Azzena GB, Michetti F, Grassi C (2008b) Dysregulation of intracellular calcium homeostasis is responsible for neuronal death in an experimental model of selective hippocampal degeneration induced by trimethyltin. J Neurochem 105:2109–2121. CrossRef Medline

Podda MV, D'Ascenzo M, Leone L, Piacentini R, Azzena GB, Grassi C (2008) Functional role of cyclic nucleotide-gated channels in rat medial vestibular nucleus neurons. J Physiol 586:803–815. Medline

Podda MV, Leone L, Piacentini R, Cocco S, Mezzogori D, D'Ascenzo M, Grassi C (2012) Expression of olfactory-type cyclic nucleotide-gated channels in rat cortical astrocytes. Glia 60:1391–1405. CrossRef Medline

Podda MV, Leone L, Barbati SA, Mastrodonato A, Li Puma DD, Piacentini R, Grassi C (2014) Extremely low-frequency electromagnetic fields enhance the survival of newborn neurons in the mouse hippocampus. Eur J Neurosci 39:893–903. CrossRef Medline

Ripoli C, Piacentini R, Riccardi E, Leone L, Li Puma DD, Bitan G, Grassi C (2013) Effects of different amyloid β-protein analogues on synaptic function. Neurobiol Aging 34:1032–1044. CrossRef Medline

Russell CL, Semerdjieva S, Empson RM, Austen BM, Beesley PW, Alifragis P (2012) Amyloid-β acts as a regulator of neurotransmitter release disrupting the interaction between synaptophysin and VAMP2. PLoS One 7:e43201. CrossRef Medline

Selkoe DJ (2002) Alzheimer's disease is a synaptic failure. Science 298:789–791. CrossRef Medline

Shaked GM, Kummer MP, Lu DC, Galvan V, Bredesen DE, Koo EH (2006) Abeta induces cell death by direct interaction with its cognate extracellular domain on APP (APP 597–624). FASEB J 20:1254–1256. CrossRef Medline

Small DH, Maksel D, Kerr ML, Ng J, Hou X, Chu C, Mehrani H, Unabia S, Azari MF, Loiacono R, Aguilar MI, Chebib M (2007) The β-amyloid protein of Alzheimer's disease binds to membrane lipids but does not

bind to the alpha7 nicotinic acetylcholine receptor. J Neurochem 101: 1527–1538. CrossRef Medline

Snyder EM, Nong Y, Almeida CG, Paul S, Moran T, Choi EY, Nairn AC, Salter MW, Lombroso PJ, Gouras GK, Greengard P (2005) Regulation of NMDA receptor trafficking by amyloid-beta. Nat Neurosci 8:1051–1058. CrossRef Medline

Takahashi RH, Capetillo-Zarate E, Lin MT, Milner TA, Gouras GK (2010) Co-occurrence of Alzheimer's disease β-amyloid and tau pathologies at synapses. Neurobiol Aging 31:1145–1152. CrossRef Medline

Talantova M, Sanz-Blasco S, Zhang X, Xia P, Akhtar MW, Okamoto S, Dziewczapolski G, Nakamura T, Cao G, Pratt AE, Kang YJ, Tu S, Molokanova E, McKercher SR, Hires SA, Sason H, Stouffer DG, Buczynski MW, Solomon JP, Michael S, et al. (2013) Aβ induces astrocytic glutamate release, extrasynaptic NMDA receptor activation, and synaptic loss. Proc Natl Acad Sci U S A 110:E2518–E2527. CrossRef Medline

Tampellini D, Magrané J, Takahashi RH, Li F, Lin MT, Almeida CG, Gouras GK (2007) Internalized antibodies to the Aβ domain of APP reduce neuronal Aβ and protect against synaptic alterations. J Biol Chem 282: 18895–18906. CrossRef Medline

Ting JT, Kelley BG, Sullivan JM (2006) Synaptotagmin IV does not alter excitatory fast synaptic transmission or fusion pore kinetics in mammalian CNS neurons. J Neurosci 26:372–380. CrossRef Medline

Ting JT, Kelley BG, Lambert TJ, Cook DG, Sullivan JM (2007) Amyloid precursor protein overexpression depresses excitatory transmission through both presynaptic and postsynaptic mechanisms. Proc Natl Acad Sci U S A 104:353–358. CrossRef Medline

Wang HY, Lee DH, Davis CB, Shank RP (2000) Amyloid peptide Abeta(1–42) binds selectively and with picomolar affinity to alpha7 nicotinic acetylcholine receptors. J Neurochem 75:1155–1161. Medline

Wang Q, Walsh DM, Rowan MJ, Selkoe DJ, Anwyl R (2004) Block of long-term potentiation by naturally secreted and synthetic amyloid beta-peptide in hippocampal slices is mediated via activation of the kinases c-Jun N-terminal kinase, cyclin-dependent kinase 5, and p38 mitogen-activated protein kinase as well as metabotropic glutamate receptor type 5. J Neurosci 24:3370–3378. CrossRef Medline

Wei W, Nguyen LN, Kessels HW, Hagiwara H, Sisodia S, Malinow R (2010) Amyloid beta from axons and dendrites reduces local spine number and plasticity. Nat Neurosci 13:190–196. CrossRef Medline

Zepa L, Frenkel M, Belinson H, Kariv-Inbal Z, Kayed R, Masliah E, Michaelson DM (2011) ApoE4-driven accumulation of intraneuronal oligomerized Aβ42 following activation of the amyloid cascade in vivo is mediated by a gain of function. Int J Alzheimers Dis 2011:792070. CrossRef. Medline